Journal of Materials Chemistry C

ROYAL SOCIETY OF CHEMISTRY

PAPER

View Article Online
View Journal | View Issue

Cite this: J. Mater. Chem. C, 2024, 12, 2738

High-κ elastomer with dispersed ferroelectric nematic liquid crystal microdroplets†

Fan Ye,[a] Chen Yang,[a] Xinxin Zhang,[a] Xiang Huang,[a] Yongmei Zhu,[a] Satoshi Aya *[ab] and Mingjun Huang *[ab]

Received 16th December 2023,
Accepted 23rd January 2024

DOI: 10.1039/d3tc04639g

rsc.li/materials-c

Ferroelectrics with reversible spontaneous polarization are commonly employed as crucial additives or bulk components in high-κ materials. They are typically found in crystalline solid materials, such as poly(vinylidene difluoride) and inorganic ceramics. Recently, an emergent class of liquid ferroelectrics was developed, with a combination of giant dielectric constant, high polarization density, and fluidity. In this work, liquid ferroelectric microdroplets were dispersed in a polymer network to develop a stretchable high-κ elastomer for the first time. The liquid ferroelectrics exhibit high room-temperature phase stability and excellent compatibility with the polydimethylsiloxane network. The resulting composites exhibit characteristic ferroelectric-like hysteresis loops under an electric field, behaving like 'intrinsic' polymer ferroelectrics, while maintaining excellent stretchability. This simple strategy of dispersing liquid ferroelectrics is expected to significantly expand the range of material species and physical properties of ferroelectric polymers or elastomers. The developed high-κ ferroelectric composites hold tremendous potential for applications in emerging wearable electronics and next-generation soft robots.

Introduction

Recent advancements have been directed towards the development of stretchable high dielectric constant (high-κ) materials for wearable electronics[1,2] and next-generation soft robots.[3,4] Among them, ferroelectrics with reversible spontaneous polarization features are frequently utilized as key additives or bulk components toward high-κ materials.[5–9] For instance, the incorporation of ferroelectric particles into polymer elastomers provides a straightforward method to enhance the material's dielectric constant and tailor its mechanical properties.[10–12] However, traditional oxide ferroelectric ceramics with ferroelectricity originating from polar domains in a crystalline phase tend to exhibit brittleness. The high volume fraction of ceramics fillers (*i.e.*, >10 vol%), which is often necessary to significantly enhance the dielectric constant,[13] leads to a degradation in mechanical properties.[14] The inherent mismatch in mechanical properties severely diminishes flexibility, long-term durability, and stability in electrical properties.

On the other hand, polymer-based ferroelectrics, such as poly (vinylidene difluoride) (PVDF) and its derivatives, have also undergone extensive investigation.[15,16] In particular, these ferroelectric polymer materials often experience plastic deformation during stretching. Very recently, Gao *et al.* addressed this challenge by developing an intrinsically elastic ferroelectric material through slight cross-linking of plastic ferroelectric polymers, achieving a balance between crystallinity and resilience.[17] Nevertheless, the properties (*e.g.*, mechanical, electric, or optical) of high-κ materials can only be tuned within a relatively narrow range due to the limited choice of polymer chemical structure.[18] It is crucial but challenging to develop other high-κ and stretchable materials with a more versatile strategy. It is worth noting that ferroelectric behavior is also observed in chiral liquid crystalline (LC) materials.[19] Giant electrostriction has been achieved by combining the properties of ferroelectric chiral smectic LCs with those of a polymer network.[20] Unfortunately, the dielectric constant (ε_r') and polarization density (P) in chiral smectic LCs are much lower than inorganic ferroelectrics.[21–23]

In this work, we introduce a novel class of stretchable high-κ elastomer *via* incorporating dispersed ferroelectric nematic (N_F) liquid crystal microdroplets (Scheme 1). N_F LC is an emergent ferroelectric fluid, characterized by marvelous viscoelasticity, topology, and electro-optic properties.[24–27] Notably, N_F LCs exhibit a high polarization density of approximately

[a] South China Advanced Institute for Soft Matter Science and Technology, School of Emergent Soft Matter, South China University of Technology, Guangzhou 510640, China. E-mail: satoshiaya@scut.edu.cn, huangmj25@scut.edu.cn
[b] Guangdong Provincial Key Laboratory of Functional and Intelligent Hybrid Materials and Devices, Guangdong Basic Research Center of Excellence for Energy & Information Polymer Materials, South China University of Technology, Guangzhou 510640, China

† Electronic supplementary information (ESI) available: Experimental details including POM images, 3D dielectric plots, morphological images, mechanical and thermal properties, temperature-dependent dielectric spectra and temperature-dependent P–E loops. See DOI: https://doi.org/10.1039/d3tc04639g

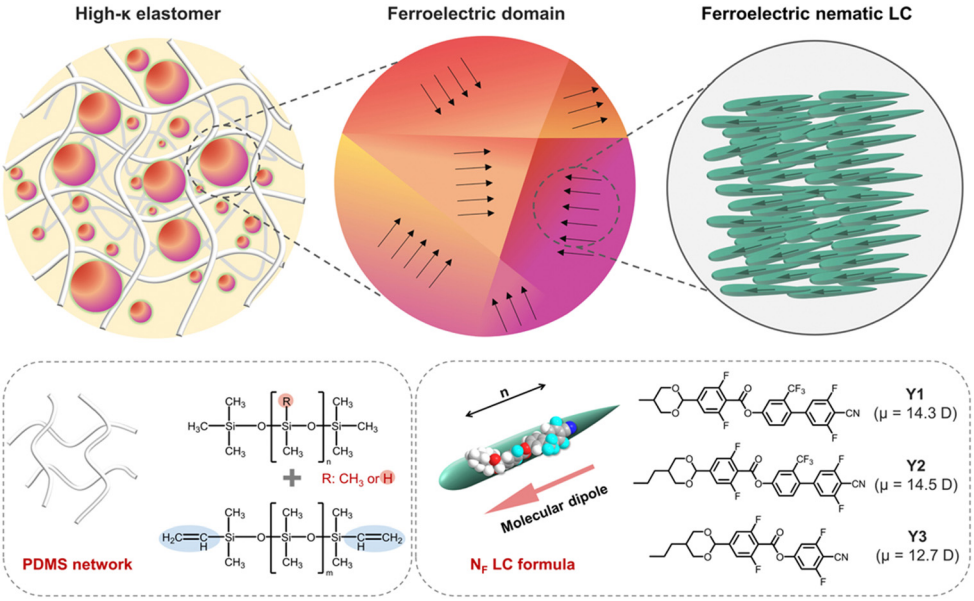

Scheme 1 High-κ elastomer featuring dispersed ferroelectric nematic liquid crystal (N_F LC) microdroplets, along with the chemical structures of PDMS network and N_F LC.

6 μC cm^{-2} and a giant dielectric constant $(\varepsilon_r' \sim 10^4@1\ \text{kHz})$, comparable to that of some inorganic ferroelectric ceramics.[28,29] Additionally, their low-voltage driving electric field response is attractive for flexible electronics applications.[30,31] The extension of the N_F phase to 'ferroelectric' polymers shows great promise.[32,33] The intriguing combination of a giant dielectric constant, high polarization density, and fluidity positions N_F LC as a desirable candidate for use as a liquid ferroelectric filler in high-κ and stretchable composite materials. Here, we optimize the formula of N_F LCs to achieve high room-temperature stability. The N_F LCs are successfully dispersed into polydimethylsiloxane (PDMS) as microdroplets, realizing a stretchable high-κ elastomer with an intrinsic ferroelectric nature.

Mingjun Huang

Mingjun Huang obtained his PhD degree in Polymer Science at the University of Akron in 2015. He then moved to the MIT Chemistry department, working on battery electrolyte material development. He started his independent career in South China University of Technology from 2019. He is currently a professor in the School of Emergent Soft Matter. He mainly focuses on soft matter functional material development within the scope of optics, electric, and energy storage. His main research projects involve: (1) liquid crystals/liquid crystal polymers with unprecedented structures and properties; (2) self-assembly of macromolecules with precise chemical structures in condensed states; (3) polymer materials for specific needs in display technology and energy storage.

Results and discussion

Preparation and characterization of N_F LC formula

Achieving room-temperature phase stability in N_F LCs has always been a critical challenge due to their tendency to crystallize at room temperature.[34] Thanks to the extensive molecular bank of N_F LCs developed in our previous work,[35,36] we were able to fine-tune the physical properties of N_F LCs through multi-component mixing. Eventually, we identified an optimized formula: an equal-ratio mixture of Y1, Y2, and Y3 molecules (Scheme 1). All these LC molecules possess large molecular dipole moments (>12 Debye), which are necessary for N_F LC phase formation. The phase behavior of this N_F LC formula was initially investigated through polarized optical microscopy (POM) in homemade 5-μm-thick slabs with planar alignment. The phase transition from isotropic (Iso) liquid to N_F phase occurred at 95 °C (Fig. 1a). Characteristic N_F LC textures covered the entire cell at 90 °C (Fig. 1b) and became smoother during cooling. A stable N_F texture persisted at 25 °C without crystallization under prolonged observation time (Fig. 1c and Fig. S1, ESI†). This phase behavior was confirmed by differential scanning calorimetry (DSC), where a single Iso-N_F phase transition peak was observed (Fig. 1d). At a scanning rate of 10.0 K min^{-1}, no crystallization peak was detected, even down to −20 °C, indicating the high stability of the N_F phase over a broad temperature range (covering general ambient temperatures).

The dynamic polarity in the N_F phase was probed by the dielectric measurement in 20 μm indium tin oxide (ITO) cells without any alignment layers upon cooling (Fig. 1e). A relatively

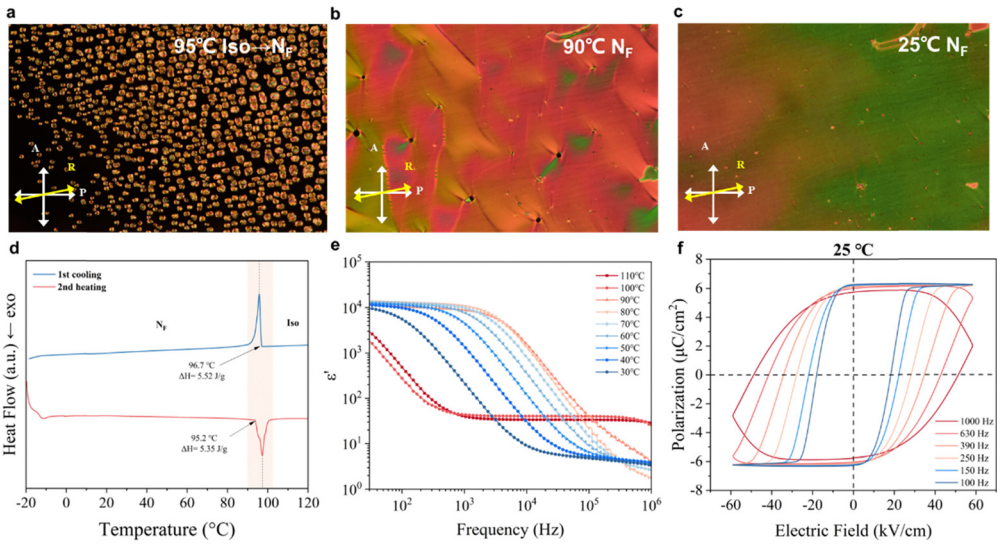

Fig. 1 (a)–(c) POM images (× 10) depict the N_F LC formula under crossed polarizers in a parallel rubbing alignment cell. *R* denotes the rubbing direction. The cell thickness is 5 μm, and the cooling rate is 5.0 K min^{-1}. (d) DSC curves at 10.0 K min^{-1}. (e) The measured ε_r' at various temperatures and their frequency dependence. (f) P–E hysteresis loops recorded at 25 °C and their frequency dependence. The P–E loops don't reach saturate polarization at a frequency higher than 150 Hz.

low apparent dielectric constant was recorded for isotropic liquids at high temperatures (100–110 °C), while a giant apparent dielectric constant ($\varepsilon_r' > 10^4$) can be obtained upon entering the N_F phase (<100 °C). The dielectric constant profiles gradually shift to a lower frequency upon cooling, indicating the slower relaxation dynamics of LC molecules. Fig. S2 (ESI†) displays 3D plots of the apparent dielectric constant ε_r' and dissipation loss as functions of frequency and temperature. Furthermore, polarization–electric field (P–E) tests were carried out to prove the ferroelectricity of the N_F LC formula. The typical parallelogram-shaped hysteresis loops are recorded in the N_F phase (Fig. 1f), confirming its ferroelectric nature. A large polarization density of ~6 μC cm^{-2} is consistent with previously reported N_F phases.[28,29,37] As the temperature increases, the P–E hysteresis loops broaden, resulting from the more significant ionic migration loss (Fig. S3, ESI†).

Preparation of ferroelectric composite elastomers

The ferroelectric composite elastomers were fabricated *via* a one-pot, *in situ* curing process, as outlined in Scheme 1. Commercial silicone rubber (Sylgard 184 PDMS) was chosen as the base material, with N_F LCs acting as ferroelectric fillers. The liquid N_F LCs were firstly dispersed into liquid precursors of PDMS (mixing the base and crosslinker at a 10 : 1 weight ratio) uniformly. As the crosslinking process preceded at elevated temperatures, PDMS networks were constructed, and N_F LCs were confined to form individual microdroplets. Note that the compatibility between PDMS and N_F LC needs to be optimized to avoid complete phase separation. The N_F LC formula shown in Scheme 1 has much better compatibility with PDMS than other reported N_F LC materials (RM734[24] or DIO[28]), and no liquid droplets were squeezed out from PDMS elastomer. The pristine PDMS (denoted as FE-0) is colorless and transparent, while the composite PDMS elastomers with dispersed N_F LC microdroplets (denoted as FE-*x*, where *x* represents the weight fraction of N_F LC in composite elastomers) become opaque (Fig. S4, ESI†). The strong light-scattering state is attributed to the mismatch of refractive indices between the polymer matrix and N_F LC droplets, similar to the phenomenon observed in polymer-dispersed liquid crystals (PDLCs).[38] POM images of 25 μm spin-coated composite films were obtained, revealing the uniform dispersion of N_F LC microdroplets with a spherical shape (Fig. S5, ESI†). The average sizes of N_F LC microdroplets increase with N_F LC concentration, as shown in Fig. 2a. The maximum average droplet size is ~8.04 ± 3.3 μm in ferroelectric elastomer when the N_F LC fraction is 40 wt% (FE-40). The DSC profiles in Fig. S6c and d (ESI†) demonstrate that all the ferroelectric composites exhibit a similar endothermic single peak between 90–100 °C, corresponding to the Iso-N_F phase transition of N_F LC. No other enthalpy changes are observed in both cooling and heating runs, confirming the good stability of the N_F phase in ferroelectric elastomers as well.

Mechanical properties

The mechanical properties of these ferroelectric composites were assessed under tensile loading (Fig. 2b). A softening trend was observed as the weight fraction of N_F LC microdroplets increased. The tensile modulus decreased from 1.61 MPa to 0.6 MPa as the weight fraction of N_F LCs increased from 0 to 40 wt% (Fig. S6a, ESI†). Despite this softening trend, the ferroelectric composites maintained similar mechanical stretchability to the pristine PDMS elastomer, with a large elongation at the break still observed at higher N_F LC concentrations, approximately ~125% of FE-40.

Effect of N_F LC on dielectric properties

Dielectric measurements of the ferroelectric composites were performed, and the films (~30 μm) were sandwiched between

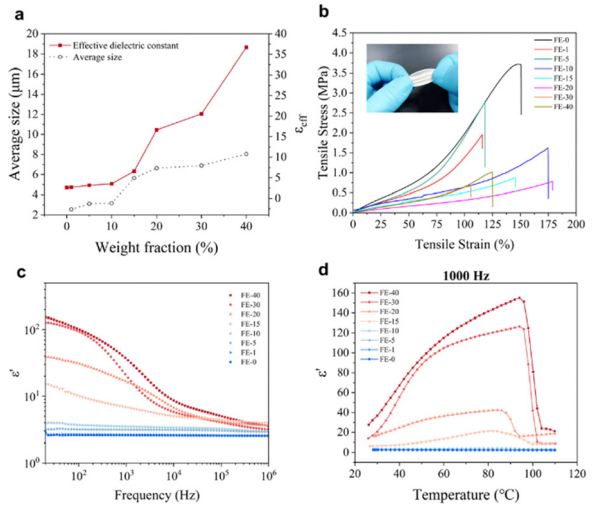

Fig. 2 (a) Average size of N_F LC droplets and effective dielectric constant (at 25 °C 1 kHz) *versus* N_F LC weight fraction in FE composites. (b) Stress–strain curves of FE composites with different N_F LC weight fractions. (c) The spectrum of the real part of the complex dielectric constant of FE composites with different N_F LC weight fractions at room temperature. (d) The real part of the complex dielectric constant *versus* temperature for different N_F LC weight fractions.

ITO glasses. Considering the high-density random-orientated N_F microdroplets in the polymer matrix, we assume the effective dielectric constant (ε_{eff}) of the N_F fillers as $\varepsilon_{eff} = (\varepsilon_{\parallel} + 2\varepsilon_{\perp})/2$ ($\varepsilon_{\parallel}$ and $\varepsilon_{\perp}$ represent dielectric constants in the directions parallel and perpendicular to the LC director respectively).[39] The εeff was notably enhanced with the increasing weight fraction of N_F LC microdroplets (Fig. 2a), especially surpassing the threshold at approximately 10 wt%. The room-temperature dielectric spectra of ferroelectric elastomers are illustrated in Fig. 2c. Considering that the N_F LC mass density (ρ) is approximately 1.3 g cm^{-3},[40] the weight fraction of FE-40 can be converted to a volume fraction of around 33.9%. The dielectric constant of FE-40 reaches about 102 at 100 Hz, marking an increase of over 40 times compared to pristine PDMS ($\varepsilon_r' \sim 2.4$). In contrast to traditional inorganic ceramic-base elastomer composites, the introduction of such a liquid ferroelectric filler not only significantly enhances the dielectric constant at a similar volume fraction but also maintains excellent stretchability even at high filling concentration.[14,41–45] The temperature-dependent dielectric constant at 1 kHz was further investigated for these ferroelectric composites (Fig. 2d). The dielectric constant increased as the temperature rose before the Iso-N_F phase transition of N_F LC. The maximum ε_r' of ~155 in FE-40 appeared near the phase transition temperature at 1 kHz, followed by a sharp decline when the temperature scanned above the Iso-N_F phase transition temperature of N_F LC. Such temperature dependence proves that the enhancement of ε_r' in ferroelectric elastomers is closely related to the highly polar domain in N_F LC microdroplets. Further details can be seen in Fig. S7 (ESI†).

Polarization of ferroelectric composite elastomers

To investigate the polarization response of ferroelectric elastomer composites under an electric field, P–E loops were measured using the same samples used for dielectric measurements. Pristine PDMS, recognized as paraelectric, exhibited a linear polarization curve with typical dielectric behavior (Fig. 3a). In contrast, ferroelectric composites exhibited significant dielectric nonlinearity, especially in high-polar electric fields. Broad hysteresis loops gradually appeared after the incorporation of N_F LC fillers, attributed to the polarization response of N_F LC microdroplets. At low filler content ($\leq$10 wt%), the remanent polarization (P_r) is higher than pristine PDMS but still maintained at a relatively low value ($<$0.04 μC cm^{-2}), as shown in Fig. 3b–d. Simultaneously, the hysteresis loop areas increased with the rising filler content, originating from the reversal of the polar domains of the N_F phase in each LC droplet. When the N_F LC weight fractions exceeded the threshold value ($>$10 wt%), an apparent parallelogram-shaped ferroelectric hysteresis loop could be obtained, accompanied by a significant increase in P_r values (Fig. 3e–h). The maximum polarization (P_m) and P_r values increased rapidly with the increasing N_F LC filler content (Fig. 3i) and exceeded 0.5 μC cm^{-2} when the N_F LC content was 40 wt%.

It is noteworthy that the dielectric nonlinearity can be observed even at a low electric field, *i.e.*, the P_m of FE-40 is 0.2 μC cm^{-2} at 20 kV cm^{-1}. The electric field required for realigning polarization is reduced by almost two orders of magnitude compared to PVDF-based ferroelectrics and their composites. Nonuniform electric field distribution will significantly impact the polarization response behaviors of dielectric composites. The local electrostatic field can be expressed as follows:[46,47]

$$\vec{E}_m^0 = \frac{\vec{E}_0}{\varepsilon_m} \quad (1)$$

$$\vec{E}_f^0 = \frac{3}{\varepsilon_f + 2\varepsilon_m}\vec{E}_0 \quad (2)$$

where $\vec{E}_m^0$ and $\vec{E}_f^0$ are derived in the Onsager local field approximation.[48] The higher the dielectric constant of the filler, the lower the electric field could be applied to the filler effectively. The resulting low effective electric field may not be strong enough to induce the polarization of the ferroelectric domain of inorganic high-κ fillers (*e.g.* $BaTiO_3$), making a low contribution to the dielectric constant enhancement of composites. Inducing effective polarization typically demands a very high poling field, leading to severe dielectric and electromechanical breakdown of the composites.[49–51] The dielectric breakdown strength was also measured as shown in Fig. S14 (ESI†). The breakdown strength decreases rapidly with increasing N_F LC weight fraction (up to 20 wt%) and reaches a relatively stable value ($>$20 kV mm^{-1}). In this work, owing to the brilliant fluidity and electric field-response sensitivity of the N_F phase, such a low electric field is sufficient to reorient the ferroelectric domain of the N_F phase, making the composites behave more likely as 'intrinsic' ferroelectrics.

Fig. S9–S13 (ESI†) presents the P–E response of ferroelectric elastomers at different frequencies and temperatures. The P–E loops notably broaden at high temperatures. With increasing

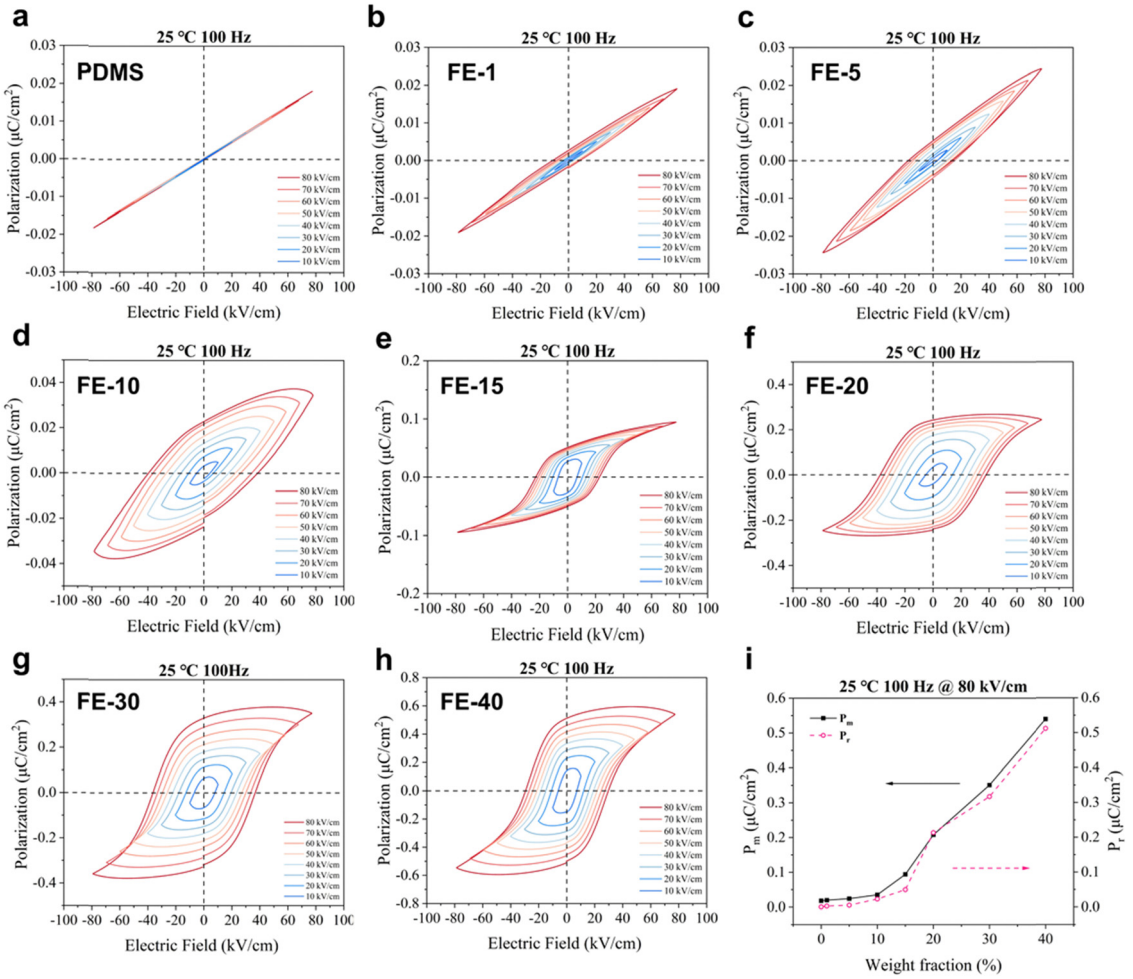

Fig. 3 (a)–(h) P–E hysteresis loops for ferroelectric elastomers with varying N_F LC contents at 25 °C, 100 Hz. (i) P_m and P_r *versus* N_F LC weight fraction at 25 °C, 100 Hz, 80 kV cm^{-1}.

temperatures, ionic migration becomes severe, and ion diffusion loss is significant during poling, particularly in the low-frequency region (below 1 kHz).[52] The characteristic ferroelectric loops vanish when the phase transition of LCs occurs, and linear dielectric behaviors are observed above 95 °C. Furthermore, the decreased coercive field (E_c) of ferroelectric composites manifests that the enhanced fluidity facilitates the polarization of N_F LCs. Such a class of polymer composite with dispersed ferroelectric fluids falls into a novel category of intrinsic polymer ferroelectrics.

AC electroluminescent devices

We next explored the application of our FE composite in the AC electroluminescent (ACEL) device as a high-κ electroluminescent layer and fabricated a demo as shown in (Fig. S15, ESI†). The maximum luminance intensity (FE-40) is increased by more than 200 times compared to pristine PDMS-based device (FE-0) at 4 V μm^{-1}. The incorporation of N_F LC can significantly improve the performance of ACEL devices at low frequency and low electric fields. Our high-κ elastomer composites exhibit promising potential for future application in novel soft electronics.

Conclusions

In this work, we introduce a high-κ polymer composite based on N_F LC which showcases a distinctive combination of fluidity and ferroelectric properties. The N_F LC mixtures exhibit remarkable room-temperature phase stability both before and after incorporation into the PDMS network. The resulting ferroelectric elastomers possess significant dielectric constant enhancement $(\varepsilon_r' > 100@100\ \text{Hz})$, surpassing other inorganic ferroelectric nanoparticle-based elastomer composites at the same filler concentration. Moreover, excellent stretchability performance is maintained even with N_F LC concentration reaching 40 wt%. Additionally, the incorporation of N_F microdroplets imparts ferroelectric characteristics to the elastomer composites, achieving a relatively high polarization of ~0.6 μC cm^{-2} at 80 kV cm^{-1}. In future endeavors, liquid crystal mesogens will be grafted onto the PDMS matrix to enhance the interaction between the polymer network and N_F LC microdroplets. The corresponding pyro- and piezoelectric properties will also be systematically studied. This innovative strategy of liquid ferroelectric-based composites will offer more potential for advancing the applications of ferroelectric polymers in novel electronic devices.

Author contributions

F. Y. and C. Y. contributed equally to this work. S. A. and M. H. designed and directed the research. F. Y., C. Y., and X. H. synthesized the materials. F. Y. and C. Y. conducted POM studies. F. Y., C. Y., and X. Z. did dielectric and ferroelectric measurements. Y. Z. conducted TGA and DSC studies. F. Y. made DFT calculation. F. Y., M. H., and S. A. wrote and revised the manuscript.

Conflicts of interest

There are no conflicts to declare.

Acknowledgements

This work is supported by the National Key Research and Development Program of China (No. 2022YFA1405000), the National Natural Science Foundation of China (NSFC No. 52273292), the Research Fund for International Excellent Young Scientists (RFIS-II; No. 1231101194), the Recruitment Program of Guangdong (No. 2016ZT06C322), the International Science and Technology Cooperation Program of Guangdong province (No. 2022A0505050006), the Fundamental Research Funds for the Central University (No. 2022ZYGXZR001).

Notes and references

1 C. Pan, E. J. Markvicka, M. H. Malakooti, J. Yan, L. Hu, K. Matyjaszewski and C. Majidi, *Adv. Mater.*, 2019, **31**, 1900663.
2 Y. J. Tan, H. Godaba, G. Chen, S. T. M. Tan, G. Wan, G. Li, P. M. Lee, Y. Cai, S. Li, R. F. Shepherd, J. S. Ho and B. C. K. Tee, *Nat. Mater.*, 2020, **19**, 182–188.
3 C. Zhang, B. Jin, X. Cao, Z. Chen, W. Miao, X. Yang, Y. Luo, T. Li and T. Xie, *Adv. Mater.*, 2022, **34**, 2206393.
4 Y. Shi, E. Askounis, R. Plamthottam, T. Libby, Z. Peng, K. Youssef, J. Pu, R. Pelrine and Q. Pei, *Science*, 2022, **377**, 228–232.
5 H. Pan, S. Lan, S. Xu, Q. Zhang, H. Yao, Y. Liu, F. Meng, E.-J. Guo, L. Gu, D. Yi, X. Renshaw Wang, H. Huang, J. L. MacManus-Driscoll, L.-Q. Chen, K.-J. Jin, C.-W. Nan and Y.-H. Lin, *Science*, 2021, **374**, 100–104.
6 B. Nketia-Yawson and Y.-Y. Noh, *Adv. Funct. Mater.*, 2018, **28**, 1802201.
7 X. Chen, H. Qin, X. Qian, W. Zhu, B. Li, B. Zhang, W. Lu, R. Li, S. Zhang, L. Zhu, F. Domingues Dos Santos, J. Bernholc and Q. M. Zhang, *Science*, 2022, **375**, 1418–1422.
8 X. Qian, D. Han, L. Zheng, J. Chen, M. Tyagi, Q. Li, F. Du, S. Zheng, X. Huang, S. Zhang, J. Shi, H. Huang, X. Shi, J. Chen, H. Qin, J. Bernholc, X. Chen, L.-Q. Chen, L. Hong and Q. M. Zhang, *Nature*, 2021, **600**, 664–669.
9 T. Tang, Z. Shen, J. Wang, S. Xu, J. Jiang, J. Chang, M. Guo, Y. Fan, Y. Xiao, Z. Dong, H. Huang, X. Li, Y. Zhang, D. Wang, L.-Q. Chen, K. Wang, S. Zhang, C.-W. Nan and Y. Shen, *Natl. Sci. Rev.*, 2023, nwad177.
10 Z.-M. Dang, M.-S. Zheng and J.-W. Zha, *Small*, 2016, **12**, 1688–1701.
11 F. E. Bouharras, M. Raihane and B. Ameduri, *Prog. Mater. Sci.*, 2020, **113**, 100670.
12 Prateek, V. K. Thakur and R. K. Gupta, *Chem. Rev.*, 2016, **116**, 4260–4317.
13 G. Zhang, Q. Li, E. Allahyarov, Y. Li and L. Zhu, *ACS Appl. Mater. Interfaces*, 2021, **13**, 37939–37960.
14 G. Gallone, F. Carpi, D. De Rossi, G. Levita and A. Marchetti, *Mater. Sci. Eng., C*, 2007, **27**, 110–116.
15 M. Guo, C. Guo, J. Han, S. Chen, S. He, T. Tang, Q. Li, J. Strzalka, J. Ma, D. Yi, K. Wang, B. Xu, P. Gao, H. Huang, L.-Q. Chen, S. Zhang, Y.-H. Lin, C.-W. Nan and Y. Shen, *Science*, 2021, **371**, 1050–1056.
16 L. Zhang, S. Li, Z. Zhu, G. Rui, B. Du, D. Chen, Y.-F. Huang and L. Zhu, *Adv. Funct. Mater.*, 2023, 2301302.
17 L. Gao, B.-L. Hu, L. Wang, J. Cao, R. He, F. Zhang, Z. Wang, W. Xue, H. Yang and R.-W. Li, *Science*, 2023, **381**, 540–544.
18 M.-H. Kwok, B. T. Seymour, R. Li, M. H. Litt, B. Zhao and L. Zhu, *Macromolecules*, 2019, **52**, 3601–3611.
19 Q. Guo, K. Yan, V. Chigrinov, H. Zhao and M. Tribelsky, *Crystals*, 2019, **9**, 470.
20 W. Lehmann, H. Skupin, C. Tolksdorf, E. Gebhard, R. Zentel, P. Krüger, M. Lösche and F. Kremer, *Nature*, 2001, **410**, 447–450.
21 A. Kocot, R. Wrzalik, J. K. Vij, M. Brehmer and R. Zentel, *Phys. Rev. B: Condens. Matter Mater. Phys.*, 1994, **50**, 16346–16356.
22 M. Brehmer, R. Zentel, G. Wagenblast and K. Siemensmeyer, *Macromol. Chem. Phys.*, 1994, **195**, 1891–1904.
23 R. Zentel and M. Brehmer, *Adv. Mater.*, 1994, **6**, 598–599.
24 R. J. Mandle, S. J. Cowling and J. W. Goodby, *Phys. Chem. Chem. Phys.*, 2017, **19**, 11429–11435.
25 R. J. Mandle, *Soft Matter*, 2022, **18**, 5014–5020.
26 N. Sebastián, L. Cmok, R. J. Mandle, M. R. de la Fuente, I. Drevenšek Olenik, M. Čopič and A. Mertelj, *Phys. Rev. Lett.*, 2020, **124**, 037801.
27 R. J. Mandle, S. J. Cowling and J. W. Goodby, *Chem. – Eur. J.*, 2017, **23**, 14554–14562.
28 H. Nishikawa, K. Shiroshita, H. Higuchi, Y. Okumura, Y. Haseba, S. Yamamoto, K. Sago and H. Kikuchi, *Adv. Mater.*, 2017, **29**, 1702354.
29 X. Chen, E. Korblova, D. Dong, X. Wei, R. Shao, L. Radzihovsky, M. A. Glaser, J. E. Maclennan, D. Bedrov, D. M. Walba and N. A. Clark, *Proc. Natl. Acad. Sci. U. S. A.*, 2020, **117**, 14021–14031.
30 O. D. Lavrentovich, *Proc. Natl. Acad. Sci. U. S. A.*, 2020, **117**, 14629–14631.
31 S. Nishimura, S. Masuyama, G. Shimizu, C.-Y. Chen, T. Ichibayashi and J. Watanabe, *Adv. Phys. Res.*, 2022, **1**, 2200017.
32 J. Li, R. Xia, H. Xu, J. Yang, X. Zhang, J. Kougo, H. Lei, S. Dai, H. Huang, G. Zhang, F. Cen, Y. Jiang, S. Aya and M. Huang, *J. Am. Chem. Soc.*, 2021, **143**, 17857–17861.
33 S. Dai, J. Li, J. Kougo, H. Lei, S. Aya and M. Huang, *Macromolecules*, 2021, **54**, 6045–6051.

34 H. Long, J. Li, M. Huang and S. Aya, *Liq. Cryst.*, 2022, **49**, 2121–2127.
35 J. Li, H. Nishikawa, J. Kougo, J. Zhou, S. Dai, W. Tang, X. Zhao, Y. Hisai, M. Huang and S. Aya, *Sci. Adv.*, 2021, **7**, eabf5047.
36 J. Li, Z. Wang, M. Deng, Y. Zhu, X. Zhang, R. Xia, Y. Song, Y. Hisai, S. Aya and M. Huang, *Giant*, 2022, **11**, 100109.
37 H. Kikuchi, H. Matsukizono, K. Iwamatsu, S. Endo, S. Anan and Y. Okumura, *Adv. Sci.*, 2022, **9**, 2202048.
38 L. Zhou, S. Liu, X. Miao, P. Xie, N. Sun, Z. Xu, T. Zhong, L. Zhang and Y. Shen, *ACS Mater. Lett.*, 2023, **5**, 2760–2775.
39 *Relaxation Phenomena*, ed., W. Haase and S. Wróbel, Springer, Berlin, Heidelberg, 2003.
40 R. J. Mandle, N. Sebastián, J. Martinez-Perdiguero and A. Mertelj, *Nat. Commun.*, 2021, **12**, 4962.
41 Z. Zhou, X. Du, Z. Zhang, J. Luo, S. Niu, D. Shen, Y. Wang, H. Yang, Q. Zhang and S. Dong, *Nano Energy*, 2021, **82**, 105709.
42 S. T. Lau, K. W. Kwok, F. G. Shin and S. Kopf, *J. Appl. Phys.*, 2007, **102**, 044104.
43 L. J. Romasanta, M. A. Lopez-Manchado and R. Verdejo, *Prog. Polym. Sci.*, 2015, **51**, 188–211.
44 J. E. Q. Quinsaat, T. de Wild, F. A. Nüesch, D. Damjanovic, R. Krämer, G. Schürch, D. Häfliger, F. Clemens, T. Sebastian, M. Dascalu and D. M. Opris, *Composites, Part B*, 2020, **198**, 108211.
45 K. K. Sappati and S. Bhadra, *IEEE Sens. J.*, 2020, **20**, 4610–4617.
46 E. Kuffel, W. S. Zaengl and J. Kuffel, *High Voltage Engineering Fundamentals*, Newnes, Oxford, 2000.
47 J. Wang, F. Guan, L. Cui, J. Pan, Q. Wang and L. Zhu, *J. Polym. Sci., Part B: Polym. Phys.*, 2014, **52**, 1669–1680.
48 E. Allahyarov, *Adv. Theory Simul.*, 2020, **3**, 2000005.
49 J. Chen, P. Jiang and X. Huang, *Encyclopedia of Polymer Science and Technology*, John Wiley & Sons, Ltd, 2021, pp. 1–44.
50 J.-Y. Pei, L.-J. Yin, S.-L. Zhong and Z.-M. Dang, *Adv. Mater.*, 2022, 2203623.
51 G. Zhang, D. Brannum, D. Dong, L. Tang, E. Allahyarov, S. Tang, K. Kodweis, J.-K. Lee and L. Zhu, *Chem. Mater.*, 2016, **28**, 4646–4660.
52 L. Yang, E. Allahyarov, F. Guan and L. Zhu, *Macromolecules*, 2013, **46**, 9698–9711.

